Design of a Passively Magnetically Stabilized System with Viscoelastic Damping Support and Flexible Elements

Josef Passenbrunner[1], Gerald Jungmayr[1] and Wolfgang Amrhein[2]
[1]Linz Center of Mechatronics GmbH, Altenbergerstrasse 69, 4040 Linz, Austria, josef.passenbrunner@lcm.at
[2] Johannes Kepler University, Altenbergerstrasse 69, 4040 Linz, Austria

***Abstract*—Using passively magnetically stabilized degrees of freedom in magnetic levitated reduces the complexity and therefore costs. In the investigated system only two degrees of freedom remain to be controlled actively. One is the rotation and the other is the axial position of the rotor, which is stabilized by an axial active magnetic bearing (AMB). However, the application of passive magnetic bearings (PMBs) features some drawbacks. One of the main problems is caused by the poor damping in PMBs, which leads to exaggerated deflection amplitudes in the resonance frequencies. This results in the necessity of external damping. One possibility is given by utilizing viscoelastic materials. But these materials show highly frequency and temperature dependent properties. Thus, only a proper model of the rotor dynamics including the nonlinear characteristics of the damping material allows for calculating the displacements of the system parts. Furthermore, also flexible parts have to be considered, if their bending modes fall within the range of operation. This article describes the rotor dynamic modeling of a passively magnetically stabilized system including the nonlinear behavior of a viscoelastic damping support as well as the consideration of the relevant flexible body modes. With this model an optimization can be performed to guarantee contact-free operation. Finally, the analytical model is verified by measurement.**

I. Introduction

Passively magnetically stabilized systems offer the possibility to design cost-efficient magnetically levitated systems. Using PMBs to stabilize the radial and tilting degrees of freedom and one AMB for the axial movement, the complexity of a magnetically levitated system can be reduced. Thereby, the demand for power electronics and position sensors is minimized. The main drawback of PMBs is the poor damping, which leads to exaggerating deflections when passing the rigid body resonances during the run up process. So additional damping has to be induced in the system. A possibility is offered by viscoelastic materials which meet the target of low costs. However, viscoelastic materials show a very frequency- and temperature-dependent stiffness and damping. For the design of such a system, the occurring deflections due to the rotor dynamics have to meet certain restrictions, so that no contact between the rotor and the stator is guaranteed. This requires the derivation of the systems equations of motion in connection with a proper model of the frequency-dependent damping elements.

In section II the system setup with the used components is described. Section III determines the viscoelastic material model followed by section IV, where the derivation of the equations of motion are presented. With the derived model an optimization is performed in section V. Afterwards the optimized system is verified by measurements in section VI. At the end of this work a conclusion and an outlook is given.

II. System Setup

Figure 1 shows the composition of the magnetically levitated system. The radial directions and accordingly the tilting of the rotor are stabilized by two radial permanent magnet (PM) ring bearings. These bearings are of repulsive type and use axial magnetized magnets which are easy to produce and lower the costs of the bearings. Furthermore, this configuration features the opportunity of easy magnet stacking [1] to achieve higher bearing stiffness with the same cross sections and thereby simplifies the rotordynamic design procedure.

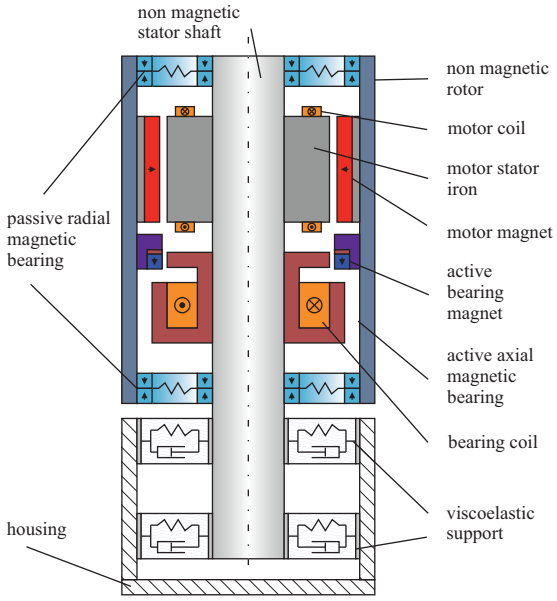

Figure 1. Setup of the investigated system

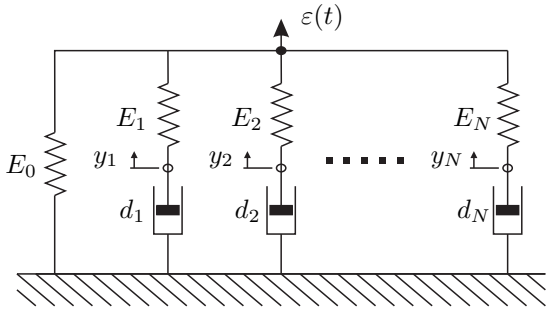

Figure 2. MAXWELL-Modell of the dynamic viscoelastic material behavior

If the bearings are not surrounded by ferromagnetic material the stabilizing radial stiffness of the bearings can be analytically calculated using [2]. This drastically simplifies the design of the bearings for the prototype because no finite element simulations are necessary.

Due to Earnshaw's theorem [3], which is adapted to passive ring bearings in [4], the destabilizing axial stiffness s_z for the used type of bearings is given by

$$s_z = -2 \cdot s_r, \tag{1}$$

whereby s_r describe the stabilizing radial stiffness.

Hence, at least one direction has to be stabilized actively. To control the unstable direction an axial AMB is placed between the two radial PMBs. Thereby the necessary relative rotor position is measured by an eddy current displacement sensor described in [5], [6]. Moreover, the motor, to drive the rotor, is situated between the PMBs. Consequently, this design leads to a relatively long stator shaft. Due to limitations of the outer diameter the stator shaft features small cross sections. Thus, its bending frequencies have to be considered in the rotordynamic design.

To support the system and add damping to radial oscillations, the stator is mounted on the housing with two circular viscoelastic damping elements.

III. MODEL OF THE VISCOELASTIC SUPPORT

Viscoelastic materials feature a frequency dependent behavior of the stiffness and damping values. To describe the characteristics of such materials often a generalized Maxwell model is used [7], [8]. As shown in Fig. 2, the model consists of a single spring with the equilibrium modulus E_0. This spring describes the material response after infinite time. A collection of Maxwell units in parallel, which consist of a single spring and a single damper connected in series, reproduce the frequency dependency by adding different time constants τ_n. In the frequency domain for harmonic excitations a representation with a complex modulus

$$E(\omega) = E'(\omega) + jE''(\omega) \tag{2}$$

is useful. Thereby, E' stands for the storage module and E'' for the loss module. The quotient gives the loss factor

$$\eta = tan\delta = \frac{E''}{E'}. \tag{3}$$

Converted to the Prony parameters [9] of the generalized Maxwell model the components of the complex modulus result in

$$E'(\omega) = E_0 + \sum_{n=1}^{N} E_n \frac{\omega^2\tau_n^2}{1+\omega^2\tau_n^2} \tag{4}$$

and

$$E''(\omega) = \sum_{n=1}^{N} E_n \frac{\omega\tau_n}{1+\omega^2\tau_n^2} \tag{5}$$

with the time constants $\tau_n = \frac{d_n}{E_n}$.

In addition, the Maxwell model uses y_n inner states. The main advantage of this model is that it can be described by a system of linear differential equations and thereby can be easily included in the overall system model.

A. Determination of Material Parameters

To describe the thermo-viscoelastic behavior usually master curves are used [9]. Thereby, the theory of temperature-time-correspondence is applied to combine measurements at different temperatures and draw conclusions to other frequencies. The basic approach is depicted in Fig. 3.

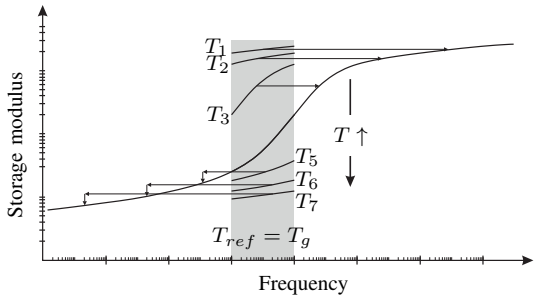

Figure 3. Application of the temperature-time-correspondence

Due to the theory the material shows the same storage modulus at a temperature T_1 and frequency f_1 as well as at a temperature T_2 and a scaled frequency f_2 according to

$$E(f_1, T_1) = E(f_1 \cdot a_{T_{2-1}}, T_2) = E(f_2, T_2) \tag{6}$$

with the shift factor $a_{T_{2-1}}$. If unfilled elastomers are used, the kinetic-theory-factor [10] has to be applied which is obtained of the theory of entropy elasticity. Thereby, the storage modulus is shifted to the reference temperature T_r using

$$E(T_r) = \begin{cases} E(T_m) * \underbrace{\frac{T_r}{T_m}}_{k_T} * \underbrace{\frac{\rho_r}{\rho}}_{\approx 1} & T_m \geq T_g \\ E(T_m) & T_m < T_g \end{cases} \tag{7}$$

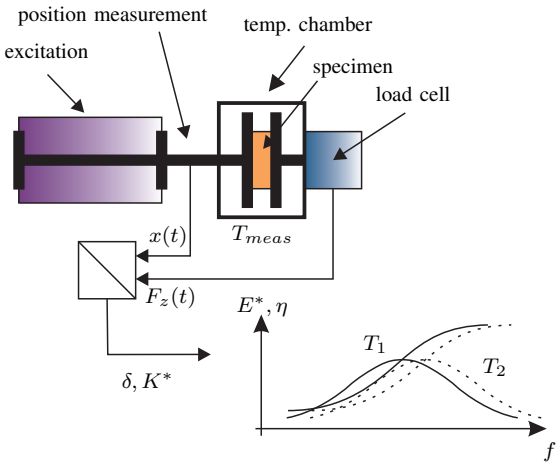

Figure 4. Scheme of employed measuring method for the viscoelastic materials

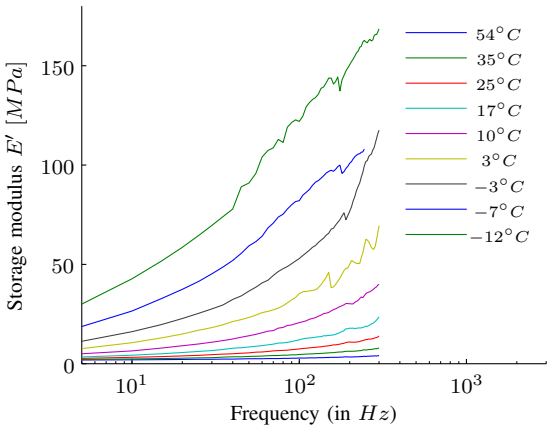

Figure 5. Storage modulus of the measured isotherms

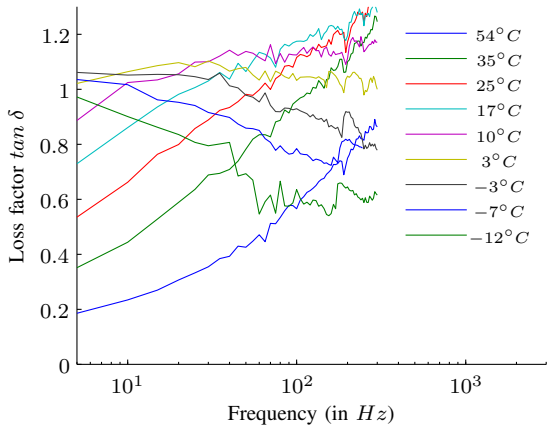

Figure 6. Loss factor of the measured isotherms

with T_m as measured temperature and the glass transition temperature T_g. The factor ρ_r/ρ normalizes the specific volume at a temperature T to the reference temperature T_r.

Master curve data is hardly provided from manufacturers and even if available it is essential to know the exact measurement conditions. For example a measurement under precompression shows a different behavior then without. Hence, it was decided to measure the data on our own. The measurement principle looks simple. However, it is a very complex task. In Fig. 4 the scheme of the employed measuring method is shown. It is based on the so called DMTA (Dynamic-Mechanic-Temperature-Analysis).

A specimen is excited at different temperatures by a harmonic deformation $x(t)$ at various frequencies. In the process the force reaction $F(t)$ is measured by a load cell. Thereby, the ratio between force and displacement reflects the stiffness of the material. Due to dissipation effects a phase shift δ between the force and the displacement signal occurs, which represents the damping capability of the material. The measurement represent the so-called isotherms. Thereafter, the measured stiffness values [11] have to be converted to the material significant storage modulus E' using the geometric parameters of the specimen. In Fig. 5 and 6 the measured isotherms of a selected butyl rubber with a hardness of Shore A40 are depicted. It can be seen that the storage modulus is increasing with decreasing temperature. However, the loss factor shows a maximum value at certain temperatures and frequencies.

For this material also data from the manufacturer is available. It was observed that the measured data shows a 50% higher stiffness and a 30% lower loss factor compared to the given data of the manufacturer. That prooves the difficulty to get proper material specifications. The isotherms are afterwards shifted using equation (6) and (7) so that the resulting stiffness and loss factor curves show a smooth gradient. There are other possibilities to shift the data which are based on physical material principles, but in our case the individual shift leads the best results. Basically the procedure to find the optimal shift parameters and consequently the identification of the Prony-parameters requires the solution of a nonlinear minimization problem. This is done using an genetic algorithm varying the shift parameters and determineing the Prony-parameters by minimizing the mean square deviation. The results are depicted in Fig. 7. The fitted model shows a very good compliance with the measured data.

IV. Rotordynamic Model

In the considered system high unbalances of the rotor can appear by an additional mass, which is placed on the rotor. So a very important aspect is the relative deflection between the stator and the rotor in the PMB planes. To determine the movement of the system bodies the equations of motion have to be derived. Due to the planned system setup, the stator part holding the AMB, the motor and the upper PMB, will evolve into a thin shaft. Therefore, it is obvious that the bending of this part will influence the system behavior. The equations of motion are conducted by using the principle of the projection equation [12], which projects the (generalized) forces into the

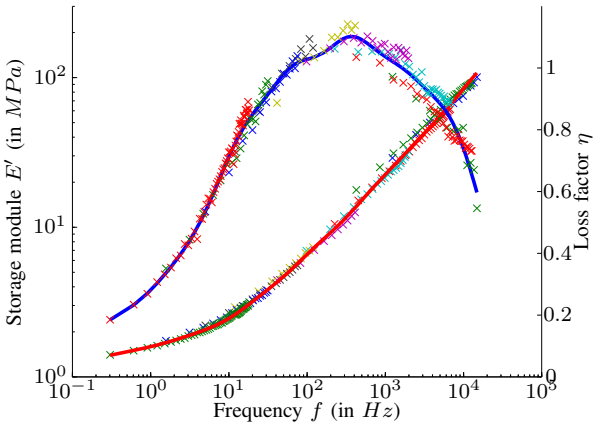

Figure 7. Fitted curves of the storage modulus (red) and the loss factor (blue) in comparison to the measured data (x), whereby the colors mark different measurement temperatures.

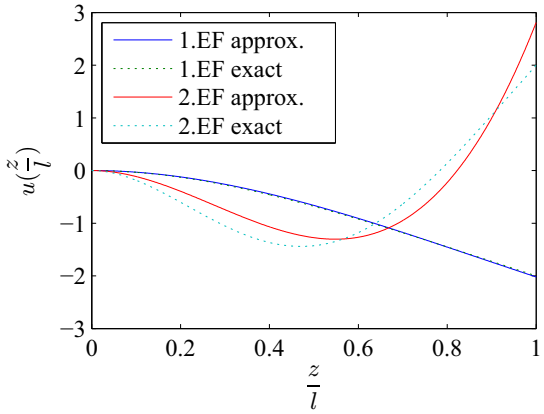

Figure 8. Comparison of the exact and approximated solution of the semibeam bending

unconstrained space, where the motion takes place. They are given by

$$\sum_{i=1}^{N}\left[\left(\frac{\partial_R \mathbf{v}_{si}}{\partial \dot{\mathbf{q}}}\right)^T\left(\frac{\partial_R \boldsymbol{\omega}_{si}}{\partial \dot{\mathbf{q}}}\right)\right]\left[\begin{matrix}({}_R\dot{\mathbf{p}} + {}_R\tilde{\boldsymbol{\omega}}_{IR}\,{}_R\mathbf{p} - {}_R\mathbf{f}^s)_i\\ ({}_R\dot{\mathbf{L}} + {}_R\tilde{\boldsymbol{\omega}}_{IR}\,{}_R\mathbf{L} - {}_R\mathbf{M}^s)_i\end{matrix}\right] + \left(\frac{\partial V}{\partial \mathbf{q}}\right)^T + \left(\frac{\partial R}{\partial \dot{\mathbf{q}}}\right)^T = 0, \tag{8}$$

with ${}_R\mathbf{v}_{si}$ and ${}_R\boldsymbol{\omega}_{si}$ describing the bodies velocities and angular velocities and ${}_R\mathbf{p}$ and ${}_R\mathbf{L}$ representing the impulse and angular momentum in the reference system R. Thereby,

$$\left(\frac{\partial_R \mathbf{v}_{si}}{\partial \dot{\mathbf{q}}}\right)^T \quad \text{and} \quad \left(\frac{\partial_R \boldsymbol{\omega}_{si}}{\partial \dot{\mathbf{q}}}\right)^T \tag{9}$$

represent the Jacobian matrices and the therms

$$\left(\frac{\partial V}{\partial \mathbf{q}}\right)^T \quad \text{and} \quad \left(\frac{\partial R}{\partial \dot{\mathbf{q}}}\right)^T \tag{10}$$

are used to consider potential forces (e.g. springs, dampers, elastic potential and gravitation). ${}_R\mathbf{f}^s$ and ${}_R\mathbf{M}^s$ constitute forces and moments acting on the center of mass.

The rotor is modeled as rigid body, whereas the stator is split into a rigid lower part and a flexible upper part. The mass of the AMB and the motor are integrated into the rigid part of the stator to reduce the complexity of the model. The mass of the upper PMB is modeled as a point mass. As flexible beam model a Ritz approach based on a cubic function $u(z) = a_0 + a_1 z + a_2 z^2 + a_3 z^3$ is used for the displacement. In Fig. 8 the comparison of the exact and approximated solution of bending a semibeam is shown. As it can be seen, the cubic approach gives a very good representation of the first bending mode which is most decisive for the investigated system.

To integrate the viscoelastic behavior the dynamic system model with the states $\mathbf{z}_r$ has to be extended with the inner states of the material model

$$\mathbf{z} = \left[\begin{array}{c|c} \mathbf{z}_r & \overbrace{\mathbf{y}_i\ \boldsymbol{\upsilon}_i}^{\mathbf{z}_i} \end{array}\right]^T. \tag{11}$$

There $\mathbf{y}_i$ are the translational and $\boldsymbol{\upsilon}_i$ the rotational inner states. The first order system is then given by

$$\begin{bmatrix}\mathbf{E} & \mathbf{0} & \mathbf{0}\\ \mathbf{0} & \mathbf{M}_c & \mathbf{0}\\ \mathbf{0} & \mathbf{0} & \boldsymbol{D}_i\end{bmatrix}\begin{bmatrix}\dot{\mathbf{z}}_r\\ \dot{\mathbf{z}}_r^p\\ \dot{\mathbf{z}}_i\end{bmatrix} + \begin{bmatrix}\mathbf{0} & \text{-}\mathbf{E} & \mathbf{0}\\ \mathbf{K}_c & \mathbf{D}_c + \mathbf{G}_c & \mathbf{K}_{ic}\\ \mathbf{K}_{ci} & \mathbf{0} & \mathbf{K}_i\end{bmatrix}\begin{bmatrix}\mathbf{z}_r\\ \mathbf{z}_r^p\\ \mathbf{z}_i\end{bmatrix} = \mathbf{0} \tag{12}$$

with the transformation $\dot{\mathbf{z}}_r = \mathbf{z}_r^p$. The transformation in a first order system is not trivial, because the inner states are massless and thus the mass matrix $\mathbf{M}$ is basically not invertible. As the inner states are only present in the first derivative only the general states $\mathbf{z}_r$ have to be transformed. The system of the inner states can be included afterwards.

Figure 9 shows the effect of the flexible stator shaft of a designated system if different shaft materials are used. In the top PMB the deflections in the first resonance are increasing with softer material. Furthermore, the bending frequency is situated in the operation range which is up to $500Hz$.
It is our aim to design a system meeting the objective of a maximum deflection of $500\ \mu m$ in both PMBs to prevent contact with the fault bearings considering an unbalance of $20\ gmm$. To achieve this goal the stiffness and the position of the PMBs and the damping elements can be varied and optimized.

As seen in Fig. 9 the stator shaft material has a huge influence on the relative rotor deflections in the first bending mode. Due to the required space for the AMB, the motor and the position sensor system, the minimum stator shaft length is given with $116\ mm$ as used in Fig. 9. For this reason the only suitable material for the shaft, that meets the requirements of a maximum deflection in the PMB planes of $500\mu m$, is steel.

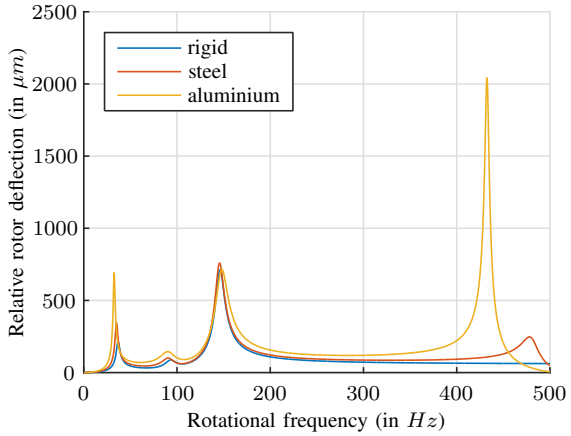

Figure 9. Relative rotor deflection at the upper PMB with different rod materials of a not optimized system

TABLE I
MAIN PARAMETERS OF THE INVESTIGATED SYSTEM

Description	Variable	Value	Unit
Rotor			
Mass of rotor	m_r	474	g
Polar moment of inertia	J_{rp}	$1.1e^{-4}$	kgm^2
Diametrical moment of inertia	J_{rd}	$4.74e^{-3}$	kgm^2
Stator			
Mass of stator	m_s	373	g
Diametrical moment of inertia	J_{rd}	$8.2e^{-4}$	kgm^2
PMB's			
Stiffness of upper PMB	$k_{r,upper}$	25700	N/m^2
Stiffness of lower PMB	$k_{r,lower}$	38100	N/m^2
Damping elements			
Outer damping elements diameter	$d_{o,DE}$	36	mm
Inner damping elements diameter	$d_{i,DE}$	23	mm

V. OPTIMIZATION

In the first optimization a given system setup was used and only the position and dimensions of the viscoelastic damping elements were optimized by minimizing the relative rotor deflections in the PMB planes. For the optimization a toolbox, developed at the Linz Center of Mechatronics (LCM), including a genetic algorithm was used, which is described in detail in [13]. In Table I the main fixed parameters of the system setup are given. The mass of the rotor includes an additional mass which is subsequently mounted on the rotor. The parameters of the optimization with their parameter range are shown in Table II.

For the excitation two different unbalances with an unbalance value of $20gmm$ are placed. They are located at the top and the bottom of the rotors linked part which will be responsible for the excitation. In case of the materials variation, different optimizations have to be conducted, because the genetic algorithm shows problems with discrete variable states. Finally, it turned out that the employment of two different materials leads to the best results. For the bottom element the material with a hardness of Shore A40, which was measured, is preferable. For the upper damping element a softer material should be used. But for this material only the manufacturer data is available leading to an uncertainty since the material plays a major role for the rotor dynamics. In Fig. 10 the Pareto front of the optimization is depicted.

It can be seen that the relative rotor deflections can be minimized to a value much smaller then the PMB airgap of 500 μm. This proves the high potential of elastomer materials. The optimized values for the damping elements are summarized in Table III.

TABLE II
VARIABLES FOR THE OPTIMIZATION

Description	Variable	min.	max.	Unit
Height of upper element	$h_{u,upperDE}$	5	20	mm
Height of lower element	$h_{l,upperDE}$	5	20	mm
Position of upper element	$l_{u,upperDE}$	-30	-50	mm
Position of lower element	$l_{l,upperDE}$	-50	-100	mm
Material of upper element	Shore A40, Shore A20			
Material of lower element	Shore A40, Shore A20			

TABLE III
OPTIMIZED VARIABLES

Variable	Value	Chosen	Unit
$h_{o,upperDE}$	9.6	10	mm
$h_{l,upperDE}$	5.01	5	mm
$l_{o,upperDE}$	-31.6	-32	mm
$l_{o,upperDE}$	-97.2	-97	mm
Material of upper element	Shore A20		
Material of damping element	Shore A40		

VI. VERIFICATION

To verify the system model a prototype was build with the optimized damping elements. To ensure a nearly comparable initial situation to the simulation the rotor without the linked part was first balanced. Afterwards defined unbalances as given

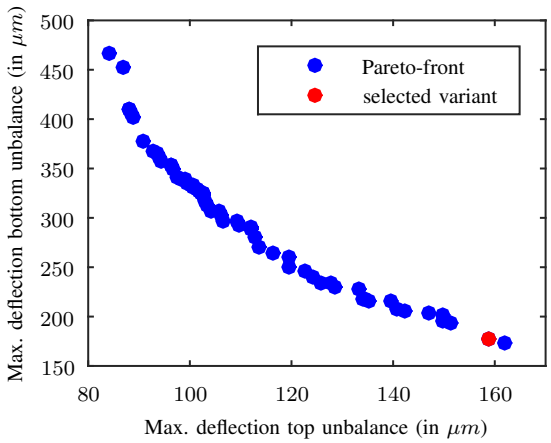

Figure 10. Pareto-front of optimization according the maximum deflections arising due to the specified unbalances

TABLE IV
VERIFICATION UNBALANCES

	Position	Value	Unit
Unbalance1	upper balance plane	7.6	gmm
Unbalance2	lower balance plane	5.6	gmm

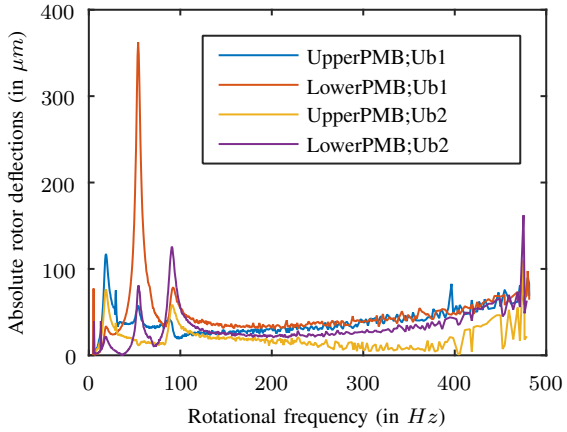

Figure 11. Measured deflections of the system according to applied unbalances as given in Table IV

TABLE V
PARAMETERS OF THE VARIFIED ROTOR

Description	Variable	Value	Unit
Mass of Rotor	m_r	365	g
Polar moment of inertia	J_{rp}	$9.32e^{-5}$	kgm^2
Diametral moment of inertia	J_{rd}	$2.46e^{-3}$	kgm^2

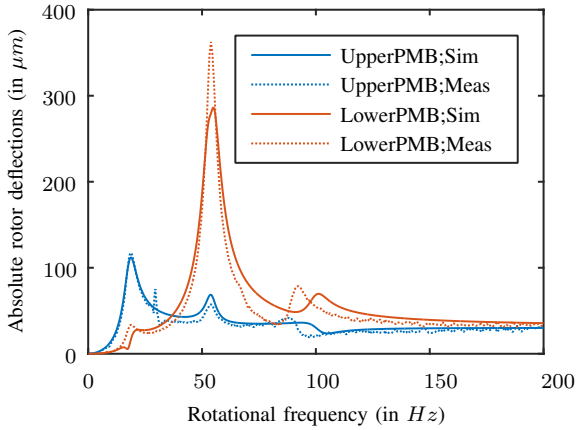

Figure 12. Comparison of the measured and simulated absolute rotor deflections at the upper and lower PMB planes with unbalance 1

in Table IV were placed at two specified positions. As it is not possible to measure the relative deflections directly, only the absolute rotor movement is compared. The measurements are conducted using laser triangulation sensors with a sample time up to 100 kHz and a resolution of 25 nm. So also high rotational speeds can be quantified with high resolution.

To eliminate the effects of the rest unbalance the deflections of the balanced rotor were subtracted from the deflections with the defined unbalances. It must be noted that this subtraction has to be performed considering the phases of the measured data properly and is permitted assuming a linear behavior of the system.

In Fig. 11 the measured absolute rotor deflections in the PMB planes related to the rotational rotor frequency f is shown. It can be noticed that the highest displacement is occuring in the lower PMB due to the unbalance in the upper balance plane. The difference to the low optimized deflections shown in Fig. 10 is caused by the lower rotor mass which has an negative influence on the system adjustment as shown in [14].

Thus, the measured rotor displacements need to be compared with adapted simulation results. For this the rotor has to be modified to characterize the one in the measured system. Without the additional mass of the linked part the rotor features the data given in Table V.

Comparing the adapted simulation with the measurement revealed that the rigid body modes of the reals system are situated at lower frequencies. That indicates a system featuring a lower overall stiffness. To identify the deviance first the stiffness of the PMBs are investigated. In a separated measurement of the PMBs it turned out, that the stiffness is 20% lower than calculated. This is due to a lower PM remanent flux density, which is confirmed with a dipole measurement of the PM rings. Furthermore, it indicates that the material of the upper damping element offers a lower stiffness, either. However, the third rigid body mode remains to be higher in the simulation. In Figs. 12 and 13 the comparison of the adjusted simulation is presented. The frequency range is limited to 200 Hz since the bending of the stator shaft is hardly apparent. The deflections show a very good compliance to the measurements even considering the high potential for uncertainty.

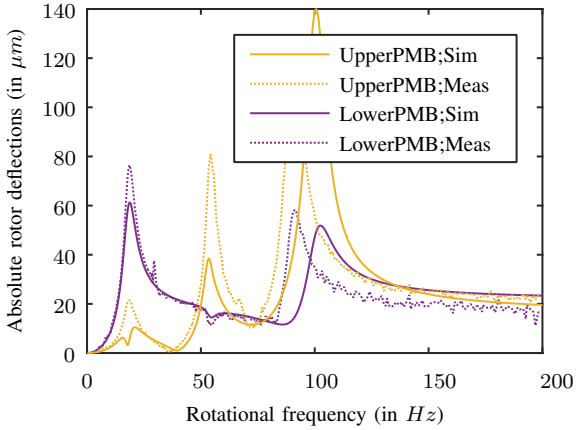

Figure 13. Comparison of the measured and simulated absolute rotor deflections at the upper and lower PMB planes with unbalance 2

The difference in the third rigid body mode implies an even softer behavior of the system. This could be generated from the lower stator part (modeled as rigid body), featuring a certain flexibility in reality. Furthermore, the disregard of the AMB and the motor featuring a negative stiffness will contribute the given characteristic.

VII. Conclusion and Outlook

As conclusion it can be said that with the introduced model it is possible to estimate the occurring deflections of passively magnetically stabilized system with viscoelastic damping support in a sufficient way. Thus, it gets possible to design magnetically levitated low cost systems and thereby widen the possibilities of application. However, a explicit knowledge of the behavior of the viscoelastic materials is essential which requires very time-consuming measurement.

To improve the accuracy of the deducted model further investigations on the behavior of the unmeasured material are intended to determine the necessary low stiffness in the verification. Also the negative stiffnesses of the motor and the AMB are feasible sources for the error in the eigenfrequencies and should be investigated in the further development.

Acknowledgment

The presented research work has been supported by the Linz Center of Mechatronics GmbH (LCM), which is part of the COMET/K2 program of the Federal Ministry of Transport, Innovation and Technology and the Federal Ministry of Economics and Labor of Austria. The authors would like to thank the Austrian and Upper Austrian Government for their support.

References

[1] R. Moser, J. Sandtner, and H. Bleuler, "Optimization of repulsive passive bearings," in *IEEE Trans. on Magnetics*, vol. 42, no. 8, August 2006, pp. 2038–2042.

[2] H. Lang, "Fast calculation method of forces and stiffnesses of permanent-magnet bearing," in *8th International Symposium on Magnetic Bearings*, Mito, Japan, 2002.

[3] S. Earnshaw, "On the nature of molecular forces which regulate the constitution of the luminiferous ether," *Transaction of the Cambridge Philosophical Society*, vol. 7, London, UK, 1842.

[4] W. Braunbeck, "Freischwebende Körper im elektrischen und magnetischem Feld," *Zeitschrift Physik*, vol. 112, pp. 753–763, 1939.

[5] J. Passenbrunner, G. Jungmayr, M. Panholzer, S. Silber, and W. Amrhein, "Simulation and optimization of an eddy current position sensor," in *PEDS 2015, 11th IEEE International Conference on Power Electronics and Drive Systems, Sydney, Australia, June 9 - 12*, Jun 2015.

[6] J. Passenbrunner, S. Silber, and W. Amrhein, "Investigation of a digital eddy current sensor," in *IEMDC, IEEE International Electric Machines and Drives Conference, Coeur d'Alne, Idaho, USA, May 10-13*, March 2015.

[7] A. Bormann, "Elastomerringe zur Schwingungsberuhigung in der Rotordynamik - Theorie, Messungen und optimierte Auslegung," Ph.D. dissertation, Technische Universität Berlin, 2005.

[8] T. Osswald, *Understanding Polymer Processing*. Hanser, 2010.

[9] D. Gutierrez-Lemini, *Engineering Viscoelasticity*. Springer, 2014.

[10] R. Ecker, "Der Einfluss verstrkender Rue auf die viskoelastischen Eigenschaften von amorphen Elastomeren," in *Kautschuk Gummi Kunstoffe 21*, vol. 21, no. 6, 1968, pp. 304–317.

[11] J. D. Ferry, *Viscoelastic Properties of Polymers*, 3rd ed., J. Wiley, Ed. John Wiley & Sons Ltd, 1970.

[12] H. Bremer, *Elastic Multibody Dynamics*. Springer, 2008.

[13] S. Silber, W. Koppelstätter, G. Weidenholzer, and G. Bramerdorfer, "MagOpt - Optimization Tool for Mechatronic Components," in *ISMB14, 14th International Symposium on Magnetic Bearings, Linz, Austria*, Aug. 2014, pp. 243 – 246.

[14] E. Marth, G. Jungmayr, and W. Amrhein, "Fundamental considerations on introducing damping to passively magnetically stabilized rotor systems," *Advances in Mechanical Engineering, Vol. 8, Dez. 2016*, vol. 8, Dez 2016.